Cold Atomic Gas in the CGPS and Beyond

Steven J. Gibson[1]

[1]*Dept. of Physics & Astronomy, Western Kentucky University, 1906 College Heights Blvd., Bowling Green, KY 42101, USA*

Abstract. The Canadian Galactic Plane Survey has opened new vistas on the Milky Way, including cold hydrogen clouds that bridge a critical gap between the classical diffuse interstellar medium and the gravitationally bound molecular clouds that can form stars. The CGPS and its fellow IGPS surveys revealed these transitional clouds to be surprisingly widespread as H I self-absorption (HISA) shadows against the Galactic H I emission background. The richness of the IGPS data allows detailed examination of HISA cloud spatial structure, gas properties, Galactic distribution, and correspondence with molecular gas, all of which can constrain models of cold H I clouds in the evolving interstellar medium. Augmenting the landmark IGPS effort are new and upcoming surveys with the Arecibo 305m and Australian SKA Pathfinder telescopes.

1. Observational Context

This review is of limited scope in order to leave room for a few current results. Readers are encouraged to consult an earlier review (Gibson 2002), as well as excellent broader H I reviews by Kulkarni & Heiles (1988), Dickey & Lockman (1990), and Kalberla & Kerp (2009), still-broader ISM reviews by Wolfire et al. (1995, 2003), Cox (2005), and Snow & McCall (2006), and many other articles in these proceedings.

Neutral atomic hydrogen (H I), the dominant constituent of interstellar matter in the Galactic disk, is found in a broad range of environments, from diffuse gas with $T \sim 10^3 - 10^4$ K (the warm neutral medium = WNM) to cold clouds with $T \sim 10 - 10^2$ K (the cold neutral medium = CNM). Consequently, the H I 21cm line is used to study the structure, properties, and distribution of gas in both the ambient ISM and denser, quiescent pockets where H_2 forms, the first step toward star formation. CNM observations, the subject of this review, allow close scrutiny of (1) the atomic-to-molecular phase transition, (2) intricate cloud structure shaped by shocks, turbulence, and perhaps magnetic fields, and (3) spiral density waves that affect H I radiative transfer. The Canadian, VLA, and Southern Galactic Plane Surveys (CGPS: Taylor et al. 2003; VGPS: Stil et al. 2006; SGPS: McClure-Griffiths et al. 2005; together, "the IGPS") have transformed our view of the CNM on all of these fronts, opening the way for future work with the next generation of H I surveys.

A simple demonstration that both WNM and CNM temperature regimes exist is to compare H I absorption toward a compact continuum source with H I emission adjacent to the source. Early interferometric studies of this sort (Clark 1965; Radhakrishnan et al. 1972) showed that narrow-line emission features have matching narrow-line absorption, but broad-line emission lacks obvious absorption counterparts, except at a
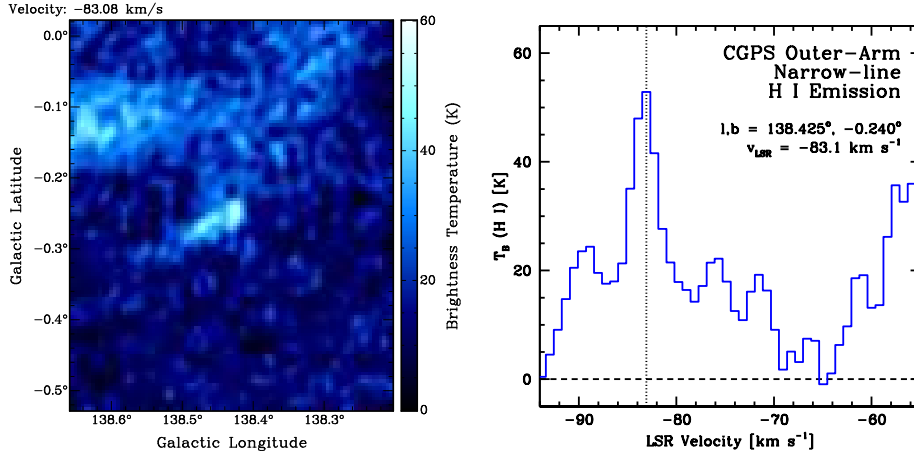
Figure 1.   CGPS narrow-line H I emission (NHIE) feature in the outer Galaxy ($d \gtrsim 6$ kpc), with ON-OFF brightness $\Delta T_b = 38$ K, line width $\Delta v = 2.8$ km/s, and angular width $\Delta \theta = 2' \gtrsim 3$ pc. Gas properties of $T_s \sim 80 - 120$ K, $\tau \sim 0.5 - 1.0$, $N_{HI} \sim 3 - 5 \times 10^{20}$ cm^{-2}, and $M_{HI} \gtrsim 25$ M$_\odot$ are consistent with measurements. No corresponding CO or FIR emission is apparent.

very weak level (e.g., Dwarakanath et al. 2002.) Two complementary physical arguments apply. One is that "warm" means "poorly absorbing": the line center optical depth varies inversely with temperature as $\tau_0 = C\,N\,/\,(T_s\,\Delta v)$, where N is column density, T_s is "spin" (excitation) temperature, Δv is the line full width at half maximum (FWHM), and $C = 5.2 \times 10^{-19}$ cm^2 K km/s for Gaussian lines (Dickey & Lockman 1990). The other argument is that "cold" means "narrow line", or less thermal broadening: $\Delta v_{therm} = 0.215\,\sqrt{T_k}$ km/s for H I, where T_k is the gas kinetic temperature (Spitzer 1978). Generally $T_s \simeq T_k$ in the CNM, but $T_s < T_k$ may occur in the WNM under some conditions (Liszt 2001). Although turbulence can broaden CNM lines significantly, it is rarely enough to confuse them with WNM lines, which form an observationally distinct population (Heiles & Troland 2003).

Whether an H I cloud is seen in emission or absorption depends on the sight line geometry. For illustration, consider the simple two-component H I radiative transfer equation (derived in Dickey 2002). Its observed brightness temperature is

$$T_B(v) \;=\; T_s\left[1 - e^{-\tau(v)}\right] \;+\; T_{bg}(v)\,e^{-\tau(v)} \;, \tag{1}$$

where v is radial velocity, T_s and $\tau(v)$ apply to the foreground cloud, and $T_{bg}(v)$ is the background brightness temperature. The cloud produces net emission if it is warm relative to the background brightness ($T_s > T_{bg}$) and absorption if cold ($T_s < T_{bg}$). The same cloud can also change from emission to absorption against a varying background. Since $\tau \propto T_s^{-1}$, WNM and CNM emission features can have similar brightness despite radically different T_s, so these phases are best distinguished by emission line width. Sufficiently narrow-line H I emission (NHIE) traces CNM unambiguously. For example, $\Delta v \lesssim 4$ km/s $\Rightarrow T_k \lesssim 300$ K, with the actual T_k probably well below this if turbulence is present. Historically only a few NHIE features were known (Knapp & Verschuur 1972; Goerigk et al. 1983), but increasingly sophisticated spectral decom-

positions have revealed more (Verschuur & Schmelz 1989; Poppel et al. 1994; Haud 2010). In the CGPS, NHIE features can be found rather easily by eye (Fig. 1).

Cold H I is more commonly identified in absorption against either a continuum source (H I continuum absorption = HICA) or other line emission (H I self-absorption = HISA). These two approaches are highly complementary. HICA is the method of choice for exploring CNM properties (e.g., Dickey et al. 2003; Heiles & Troland 2003), because it has fewer radiative transfer unknowns. One can move off the H I frequency to get T_{bg} exactly, where HISA (and NHIE) line backgrounds must be estimated. One can also move off the continuum position to see the cloud in emission, a HISA rarity (Kerton 2005). But HICA sight lines are discrete and well separated in present surveys (0.6 per deg^2 in the CGPS; Strasser & Taylor 2004), so individual clouds are often sampled only once, or missed entirely. On larger scales though, HICA sampling in the IGPS is sufficient to see Galactic structure: Strasser et al. (2007) give a beautiful longitude-velocity HICA map of spiral arms in CNM, while Dickey et al. (2009) find a surprisingly steady mix of CNM and WNM in the outer disk, where equilibrium models predict less CNM or even none due to a drop in pressure (Wolfire et al. 2003).

HISA is the preferred method for mapping detailed CNM structure in absorption (Fig. 2). Although not ubiquitous, bright H I emission is smooth and extensive enough to allow HISA shadows of CNM clouds to be imaged over large areas (Riegel & Crutcher 1972; Knapp 1974a; Wendker et al. 1983). Most bright H I is near the Galactic plane, but this is also where the bulk of the CNM is located (Cox 2005). HISA backgrounds are typically not as bright as HICA backgrounds, so the CNM sampled by HISA has a lower maximum T_s than HICA and is more focused on the coldest H I where H$_2$ formation is taking place. In fact, very narrow-line HISA in H$_2$ clouds can probe the cloud chemistry and evolutionary state (Li & Goldsmith 2003; Goldsmith & Li 2005; Goldsmith et al. 2007). Lastly, since the HISA line emission background must overlap in velocity with the absorbing cloud, HISA radiative transfer samples both the temperature and velocity fields along the line of sight, aiding Galactic structure investigations. The rest of this review discusses HISA results primarily.
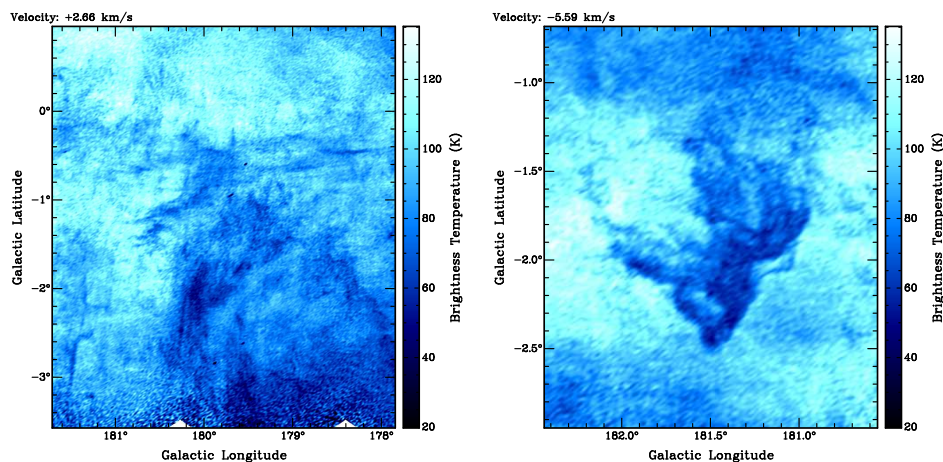

Figure 2.   Striking anticenter H I self-absorption (HISA) features in new CGPS-III data, with typical line widths $\Delta v \sim 2-3$km/s. Neither has been identified previously, except tentatively in the DRAO 26m H I survey (Higgs et al. 2005). Comparison to new FCRAO CO data is planned (see Brunt and Mottram articles, this volume).

2.   HISA in the CGPS Era

Before the CGPS, HISA was mostly used to examine H I content in molecular clouds, either in single-beam observations toward lists of objects (e.g., Knapp 1974b; Mc-Cutcheon et al. 1978) or in synthesis imaging of small areas (e.g., Landecker et al. 1980; van der Werf et al. 1989). The common presumption was that HISA gas is too cold to exist without some form of molecular cooling and shielding from the interstellar radiation field. So time-consuming HISA searches outside known dark/CO clouds were not pursued, except in position-velocity strip surveys with Arecibo (Baker & Burton 1979; Bania & Lockman 1984) and in lower-resolution maps of chance discoveries (e.g., Riegel & Crutcher 1972; Hasegawa et al. 1983). Many studies used the Maryland-Green Bank 91m H I survey (Westerhout & Wendlandt 1982), whose angular resolution was sufficient to study basic aspects of large HISA features (e.g., Fig. 3). The need for a synthesis imaging survey to detect and study HISA at smaller scales was not widely appreciated. However, such an undertaking was also impractical before the computing power and automated techniques of the 1990s (Higgs 1999).

   The CGPS was not designed as a HISA search engine, but its high angular resolution and unbiased coverage of a large area proved ideal for this purpose. New, intricate HISA clouds were found, including many without corresponding CO emission (Fig. 3; see also Gibson et al. 2000; Knee & Brunt 2001; Kerton 2005). Similar discoveries in the SGPS and VGPS came rapidly (McClure-Griffiths et al. 2001; Kavars et al. 2003; Gibson et al. 2004; McClure-Griffiths et al. 2006). All were greatly aided by the inclusion of single-dish data with the synthesis observations for full *uv* coverage. In the CGPS, comparison data in the ^{12}CO $J = 1 - 0$ line (Heyer et al. 1998) and far-infrared *IRAS* dust emission (Cao et al. 1997; Kerton & Martin 2000) were also a significant advantage. The now-common view that large, blind, high-resolution, multiwavelength surveys are worthwhile is due in no small part to the pioneering CGPS effort.
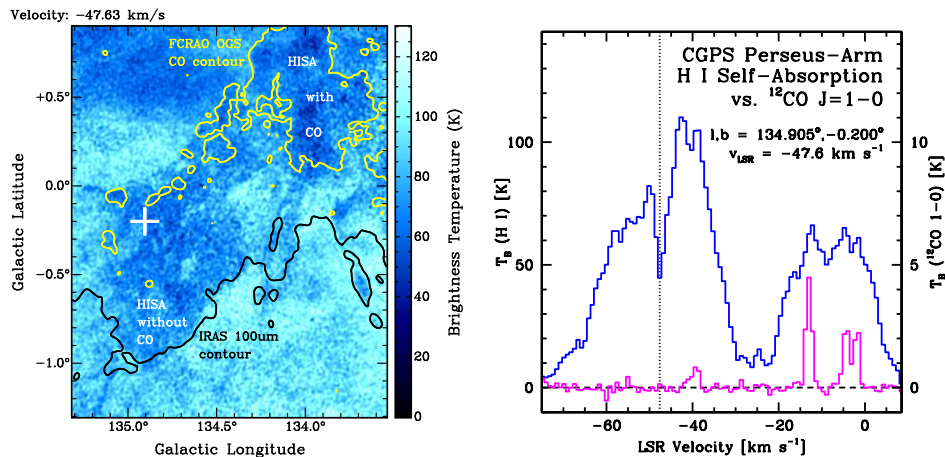

Figure 3.   CGPS Perseus-arm HISA $\sim 1°$ S of W4. *Left:* H I image with ^{12}CO (0.6 K) and FIR 100 μm (63 MJy/sr) contours. The cross marks the position of the H I and CO spectra at right. HISA extends well beyond the detected CO but has matching dust emission, suggesting H_2 untraced by CO. This HISA-CO discrepancy is large enough to be visible at $\sim 10'$ resolution (Hasegawa et al. 1983).
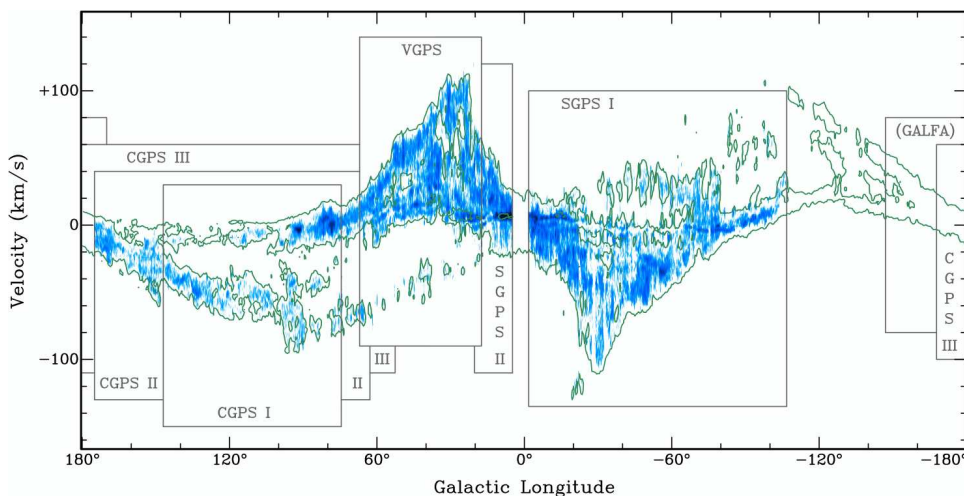
Figure 4. IGPS HISA longitude-velocity distribution over most of the Galactic disk, integrated in latitude as $\int (T_{ON} - T_{OFF})\, db$ (strong absorption is dark). Survey areas are marked. CGPS-III data are not yet included. "GALFA" = Arecibo anticenter coverage. Contours show H I emission with $T_B = 70$ K, the minimum for HISA to be detected reliably by the search algorithm. Inner-Galaxy gas has $v_{LSR} \gtrsim 0$ km/s for $0° < \ell < 180°$ and $v_{LSR} \lesssim 0$ km/s for $180° < \ell < 360°$, while gas outside the Sun's orbit occupies the other two (ℓ, v) quadrants.

3.   HISA Galactic Distribution

HISA is very common at arcminute resolution (Gibson et al. 2000; Dickey et al. 2003). The rich structure and sheer number of HISA clouds in the IGPS are too much to analyze by hand, so automated methods of feature identification and extraction were developed (Gibson et al. 2005a; Kavars et al. 2005). Reliable HISA identifications are distinguished from gaps in the general H I emission by having narrow lines, fine angular structure, and smooth, bright backgrounds. These criteria select real features that appear as coherent entities in "movies" of successive velocity channel maps in (ℓ, b, v) image cubes, often with significant kinematic structure. One can also require molecular/dust tracers for verification (e.g., Knapp 1974b), but these limit detections to the target clouds, missing the larger HISA population. Of course, the other criteria miss HISA with broader lines, weaker backgrounds, etc., but such features are hard to distinguish algorithmically from emission gaps. They can be identified by eye (Knee & Brunt 2001) but cannot be included in any population study using uniform criteria.

HISA surveys have been published for the Phase-I CGPS (Gibson et al. 2005b) and SGPS (Kavars et al. 2005), and partially for the VGPS and CGPS-II (Gibson et al. 2004, 2007). Fig. 4 shows the longitude-velocity distribution from all these surveys, with the SGPS reprocessed using the CGPS algorithm. The HISA (ℓ, v) distribution looks quite similar to its HICA equivalent (Strasser et al. 2007, Fig. 7). Weak self-absorption is found essentially everywhere that emission backgrounds are bright enough, while stronger HISA is clumped into complexes along spiral arms, tangent points, etc. Abundant outer-Galaxy HISA and HICA are present in the Perseus and Outer arms for $0° < \ell < 180°$, and in the Sagittarius and Perseus arms for $180° < \ell < 360°$ (see Fig. 5 for arm labels).

The spatial distribution of IGPS HISA clouds is a function of the conditions required to produce such cold H I and the radiative transfer geometry needed for it to self-absorb. In the outer Galaxy, where pure circular rotation allows only one distance for a given velocity, the presence of HISA requires other gas motions to provide the emission background. Turbulent eddies can make backgrounds for the scattered weak HISA, but spiral density waves are needed for the more organized strong HISA (Gibson et al. 2005b). Cold H I may arise naturally downstream of spiral arm shocks (Minter et al. 2001; Bergin et al. 2004), and colliding turbulent flows could make cold clouds on smaller scales (Vázquez-Semadeni et al. 2007), so both mechanisms that reveal cold H I as HISA may also be responsible for its creation.

In the inner Galaxy, individual spiral arms are difficult to discern (Kavars et al. 2005; Gibson et al. 2007), either because cold interarm H I is common, or because the arms themselves are less well separated in (ℓ, v). Circular rotation allows two distances per velocity here, so near-side cold H I automatically has a far-side emission background, whether in arms or not. This is probably why the inner-Galaxy HISA is more prominent and widespread. It is also the rationale behind using the detection of HISA in CO clouds to resolve near/far kinematic distance ambiguities (Jackson et al. 2002; Busfield et al. 2006; Anderson & Bania 2009; Roman-Duval et al. 2009). Such analyses presume no far-side HISA occurs, or it is "filled in" by near-side emission. The former is unlikely given outer-Galaxy HISA (see also Fig. 7), while the latter requires a conspiracy of matching foreground NHIE features. Near-side HISA may be so abundant that these caveats are minor, but they should be assessed carefully. The additional implicit assumption that HISA only arises within CO clouds is also problematic; selecting only HISA matching the shapes of CO clouds may help (Anderson & Bania 2009), but there is no guarantee of identical HISA+CO morphology (e.g., Fig. 3).

4.   HISA Relation to Molecular Gas

The IGPS HISA has a varying degree of correspondence with CO emission (Fig. 5). Close inspection of HISA in the CGPS and VGPS shows that *most inner-Galaxy HISA has matching CO, but most outer-Galaxy HISA does not*. In the SGPS, which is dominated by inner-Galaxy HISA, only $\sim$ 60% of identified HISA clouds contain CO (Kavars et al. 2005). CO without HISA is readily explained as simply lacking the requisite bright H I emission background. The reverse case of HISA without CO is more interesting, as standard CNM equilibrium models cannot explain very cold H I without molecular gas (Wolfire et al. 2003). Either the CNM models don't always apply, or some HISA clouds have H_2 untraced by CO.

HISA without H_2 might arise if a shock removed the dust grains responsible for photoelectric heating (Heiles & Troland 2003). The next-most important heat source, starlight photoionization of C I, would yield a much lower gas temperature (Spitzer 1978; Kulkarni & Heiles 1988; Wolfire et al. 1995). Oddly, such clouds might be stable as very cold H I, since the same kind of dust dominates both photoelectric heating and H_2 formation: very small grains and/or aromatic hydrocarbons (Bakes & Tielens 1994; Habart et al. 2004). Grains of this sort may be destroyed in strong shocks (O'Halloran et al. 2006; Micelotta et al. 2010). However, many shocks would be needed to account for all the weak HISA without CO. At the same time, the shocks could not be too large-scale, since many stronger HISA features have partial CO correspondences (Fig. 3). So some CO-free HISA might be explained in this way, but certainly not all.
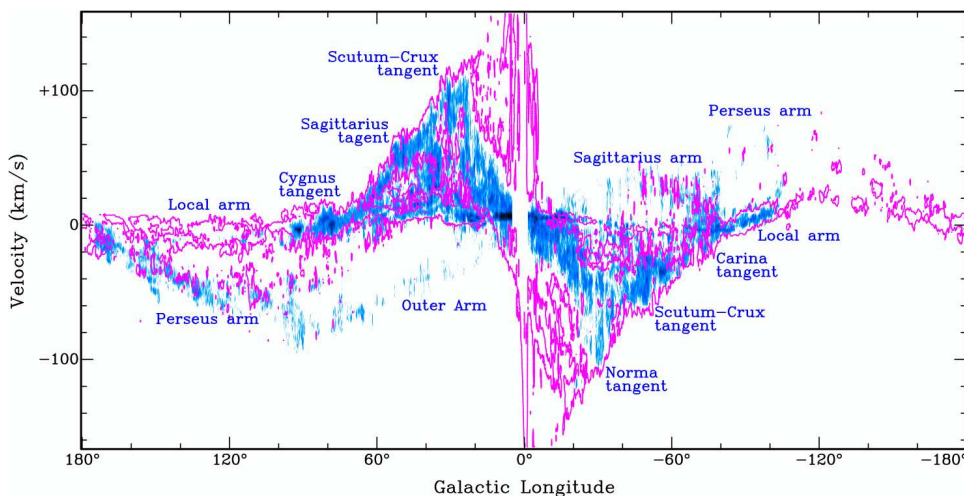
Figure 5. IGPS HISA (ℓ, v) distribution as in Fig. 4, but with Dame et al. (2001) CfA ^{12}CO $J = 1 - 0$ contours for latitude-integrated emission $\int T_B \, db = 0.4$ K deg, near the survey sensitivity limit. Relevant spiral arms and tangent points are marked.

H_2 without CO emission can occur deep in molecular cores and in H_2 cloud outer envelopes. In cold cores, CO freezes onto grain mantles (Bergin & Tafalla 2007). But this requires densities $\gtrsim 10^5$ cm^{-3}, much higher than normal HISA gas properties (Goldsmith & Li 2005; Klaassen et al. 2005), and CO would still be visible in a lower-density region surrounding the core. In molecular cloud envelopes, and diffuse molecular clouds generally, UV absorption studies show that H_2 is shielded from dissociating UV photons but CO is not for column densities of $N_H \sim 3 - 5 \times 10^{20}$ cm^{-2} (Snow & McCall 2006; Sheffer et al. 2008). In addition, both the FCRAO Outer Galaxy and CfA Composite ^{12}CO $J = 1 - 0$ emission surveys (Heyer et al. 1998; Dame et al. 2001) have sensitivity cutoffs near ~ 2 K km/s, or $N_H \sim 7 \times 10^{20}$ cm^{-2} using the CfA conversion factor. Thus, current CO emission studies are blind to H_2-dominated gas for $N_H \sim 3 - 7 \times 10^{20}$ cm^{-2}, which may include a significant fraction of the total cloud mass (Wolfire et al. 2010). H_2 in this regime has been inferred from gas property constraints in HISA clouds (Hasegawa et al. 1983; Klaassen et al. 2005; Hosokawa & Inutsuka 2007), from "infrared excess" clouds with more dust thermal radiation than their H I would imply (Reach et al. 1994; Douglas & Taylor 2007), and from "dark gas" clouds with a similar excess of proton-scattered γ-rays (Grenier et al. 2005; Abdo et al. 2010). The widespread detection of CO-free diffuse H_2 makes it a likely host for HISA.

Since many HISA clouds are near spiral density waves in longitude-velocity space, the HISA-CO relationship may be *evolutionary* rather than static. In the grand-design view of star formation, diffuse atomic gas entering a spiral arm is compressed in a spiral shock (Roberts 1969). Its sudden high density leads to rapid cooling (Spitzer 1978), H_2 condensation (Koyama & Inutsuka 2000; Bergin et al. 2004), and star formation (Roberts 1972; Heyer & Terebey 1998). This scenario has been proposed for HISA in the CGPS (Gibson 2002; Gibson et al. 2005b), VGPS (Minter et al. 2001; Gibson et al. 2007), and SGPS (Sato et al. 1992; Kavars et al. 2005) regions. In outer-Galaxy arms, the HISA traces cold H I on the near side of the arm and immediately downstream of the shock, where it is backlit by warmer H I emerging on the far side of the arm (Gibson

et al. 2005b). The HISA and CO appear poorly mixed in all the outer-Galaxy arms in Fig. 5, because (1) the HISA may form faster than the CO, or without sufficient UV shielding for CO, and (2) much of the CO may lie deeper within the spiral arm, with less H I emission behind it for illumination. Inner-Galaxy sight lines show much more CO with HISA, since all near-side clouds have far-side backgrounds (see § 3).

Excitingly, Braun et al. (2009) have recently identified "self-opaque" cold H I emission features in exquisitely sharp WSRT images of M31, which is too inclined for cold H I to appear as HISA in the same fashion as in the Milky Way. Not only do many of the opaque H I clouds lie along the edges of spiral arms near spiral shocks, but they also exhibit the same incomplete correspondence with CO as IGPS HISA.

5. Cold H I in Numerical Models

The computing power that enabled the IGPS also allowed significant advances in ISM numerical models at scales of interstellar clouds (Vázquez-Semadeni et al. 2006, 2007; Hennebelle & Audit 2007; Hennebelle et al. 2008) and spiral arms (Dobbs et al. 2006, 2008; Kim et al. 2006, 2008). While these new models are very interesting, only a few have been put in a form that can readily be compared to data from a real radio telescope (e.g., Hennebelle et al. 2007; Douglas et al. 2010). This is accomplished through "synthetic observations" of numerical models inside the computer, applying radiative tranfer to (x, y, z) grids of density, temperature, and velocity to produce (ℓ, b, v) brightness temperature grids of, e.g., H I 21cm line emission. It is natural to wonder how well CNM tracers like NHIE and HISA can be discerned in such simulations, and whether comparisons to real observations can constrain the model physics.

Gibson et al. (in prep) have made synthetic observations of 100×100 pc^2 magneto-hydrodynamic (MHD) models of gas with a wide range of densities and temperatures from Gazol et al. (2005, 2009), to see (a) under what conditions cold H I can be identified as HISA or NHIE, and (b) how well the appearances of these features under different model conditions match real HISA and NHIE clouds. As Fig. 6 shows, NHIE features are common, with amplitudes and line widths similar to CGPS NHIE (Fig. 1),
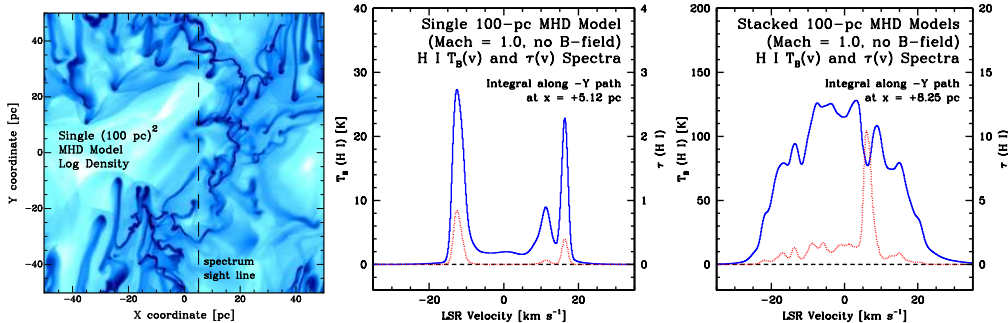

Figure 6.   *Left:* 100×100 pc^2 2-D MHD model log(density) field (0.05 pc cells). *Center:* Synthetic observed spectrum through the model. NHIE features appear as matching peaks in T_B and τ. *Right:* Synthetic spectrum from 40 concatenated models. This simulates a much larger ISM column, providing adequate backgrounds for HISA, in which T_B dips coincide with τ peaks.
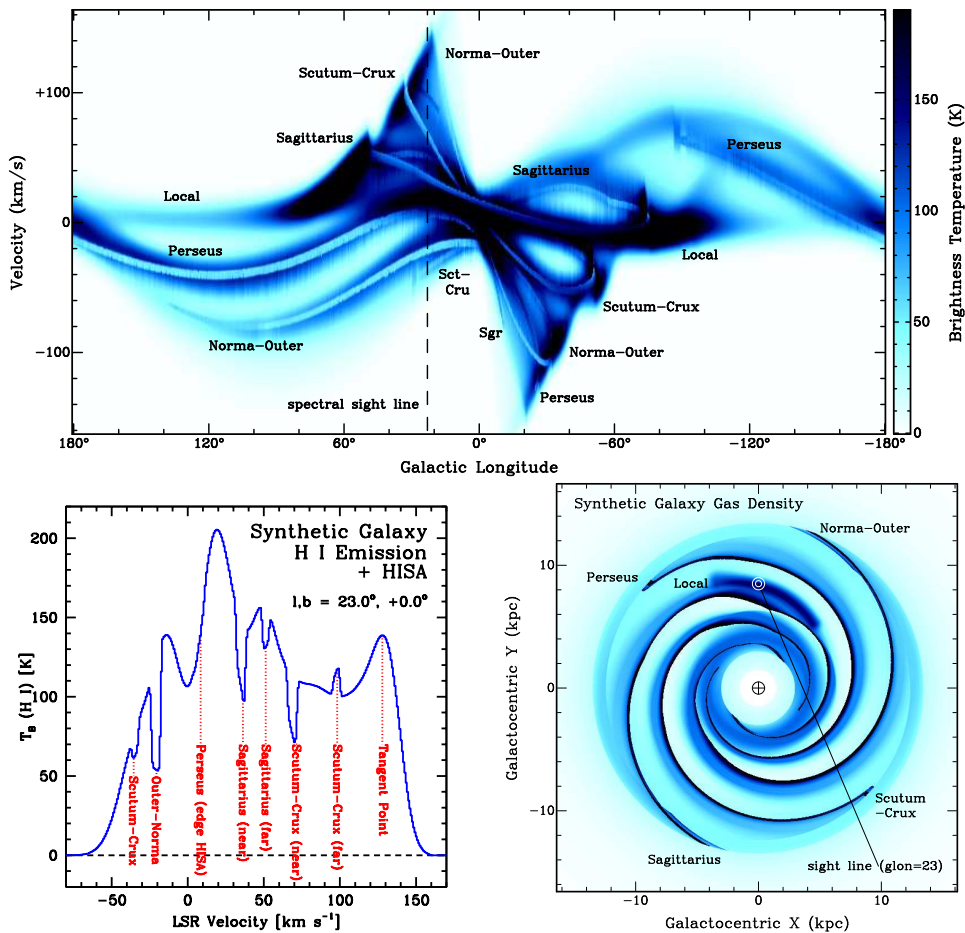
Figure 7.   *Top:* Synthetic (ℓ, v) observations of a simple 2-D Galactic H I model with cold H I downstream of spiral shocks, where it is visible as HISA (Bell & Gibson, in prep). The intensity scale is negative, so absorption appears light. *Lower Left:* Spectrum at $\ell = 23°$, showing HISA in outer-Galaxy arms and both near- and far-side inner-Galaxy arms; one Scutum-Crux arm crossing appears in NHIE. *Lower Right:* Plan-view of the model density distribution (dark is more dense).

but there is not enough H I emission background for HISA. This can be crudely addressed by observing many models end-to-end to simulate a larger region (Fig. 6), although this requires a considerable path length if the mean model density (1 cm^{-3}) is not increased. Curiously, even with many models added together, the classical WNM gas with $T > 1000$ K does not produce enough background emission by itself for the HISA to be seen. The rest of the emission comes from cooler gas, including thermally unstable gas between the equilibrium WNM and CNM regimes. Such unstable gas, predicted by prior simulations (Gazol et al. 2001), has been found in great quantity in recent HICA studies (Heiles 2001; Heiles & Troland 2003).

An alternative approach is to model the whole Galaxy, including density, temperature, and velocity variations in spiral arms. Fig. 7 shows an example of this with cold H I in bands downstream of spiral shocks (Gibson 2006; Bell & Gibson, in prep). The

arm positions and shock parameters are not intended to be exact, as the goal is merely to seek qualitative agreement with the HISA seen in the IGPS. The arm pattern is adapted from Taylor & Cordes (1993), with a Wolfire et al. (2003) global H I distribution and flat rotation curve modified by Roberts (1969, 1972) spiral shocks. Each 25 pc (x, y) model cell contains either pure WNM (T = 8000 K, $n \sim 0.5$ cm^{-3}) or pure CNM (T = 40 K, $n \sim 100$ cm^{-3}), with the latter usually confined to the major spiral arms (not the Local arm in this example). This simple model produces copious HISA in spiral arms all across the Galactic disk (Fig. 7). The WNM filling factor is fudged here (100%), but emission backgrounds are too weak to make HISA with the local value ($\sim 50\%$; Heiles & Troland 2003). As with the MHD model above, this may indicate that real HISA backgrounds arise from a mix of classical WNM gas and cooler, more opaque H I emission. For clarity, the sample model in Fig. 7 has no turbulence, nor any cold H I between arms. Experiments with different models indicate that the IGPS outer-Galaxy HISA is best explained by turbulent CNM in arms rather than random clouds throughout the disk, while inner-Galaxy HISA requires at least some interarm CNM, or arms that are less clearly separated in radial velocity (Gibson et al. 2007).

Douglas et al. (2010; Douglas, this volume) use a more sophisticated approach with 3-D (ℓ, b, v) synthetic observations of the Galactic-scale MHD models of Dobbs et al. (2008) to simulate the CGPS H I data set. They find considerable HISA in their own version of the Perseus arm and are able to track throughout the radiative transfer to determine exactly where the HISA arises and under what conditions.

6.   Magnetic Fields?

The influence of magnetic fields on ISM structure is unclear but may be significant (Kulkarni & Heiles 1988). Fig. 8 shows a possible alignment of H I emission filaments and $\vec{B}$-field direction measured from starlight polarization. The filaments are near the detection limits for 3′ smoothed CGPS data ($\Delta T_B \sim 5$ K), but those that can be isolated
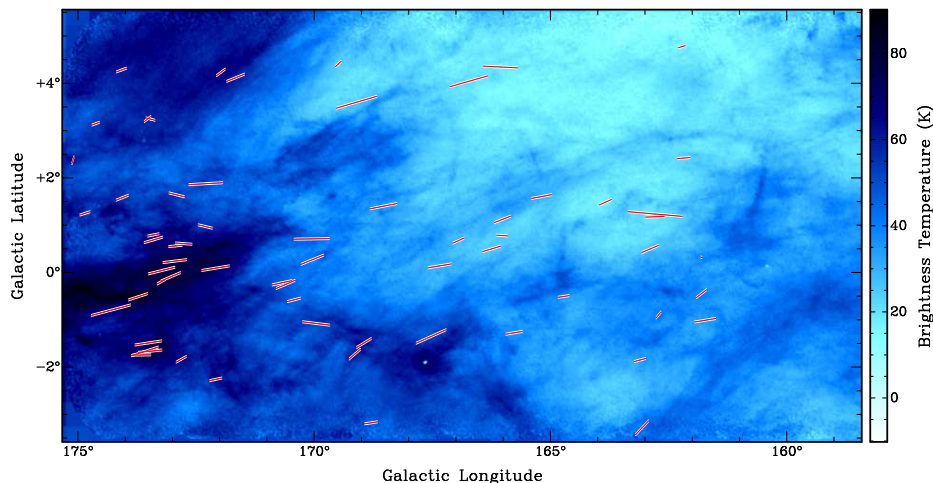

Figure 8.   CGPS H I emission filaments in local gas (v_{LSR} = +5 km/s). Lines show interstellar magnetic field direction from starlight polarization data (Heiles 2000). A line 1° long represents 5% optical polarization.

in velocity are cold ($\Delta v \sim 5$ km/s), with column densities similar to small HISA features ($N_H \sim 5 \times 10^{19}$ cm^{-2} for $\tau \ll 1$). Many such alignments are visible over the survey area. Is the field following the filaments, or vice-versa? McClure-Griffiths et al. (2006) found a similar alignment in stunning SGPS images of the Riegel & Crutcher (1972) HISA cloud. Following their analysis using the RMS scatter of position angles σ_{PA} (Chandrasekhar & Fermi 1953), the predicted CGPS mean sky-plane field strength is

$$\langle B_\perp \rangle \;=\; 63.5\,\mu\text{G}\left(\frac{10°}{\sigma_{PA}}\right)\sqrt{\left(\frac{100\,\text{pc}}{d}\right)\left(\frac{3'}{\Delta\theta}\right)\left(\frac{\Delta T_B}{5\,\text{K}}\right)\left(\frac{\Delta v_{turb}}{5\,\text{km/s}}\right)}\;. \qquad (2)$$

This is an order of magnitude more than expected for the diffuse ISM, but it's consistent with the McClure-Griffiths et al. (2006) HISA and some other cases (e.g., Andersson & Potter 2005). Could some CNM gas have strong B-fields? More sensitive Arecibo data show similar alignments for fainter filaments ($\Delta T \gtrsim 0.5$ K; J. Peek, in prep) that may probe more ordinary B-field strengths of a few μ G.

7. GALFA and Future Surveys

The IGPS surveys have transformed our view of the CNM at arcminute scales, but they are hampered by 20th-century interferometer sensitivities. Another approach is to use the Arecibo 305m telescope to map cold H ɪ with a slightly larger beam (3.4$'$) but much better sensitivity. The latter, along with installation of the ALFA 7-beam feed, has allowed better velocity sampling and more rapid mapping in the Galactic ALFA (GALFA) H ɪ survey (see Peek, this volume). GALFA targets the whole Arecibo sky ($-1.3° < \delta < 37.9°$; 32% of 4π sr), including the 1st quadrant and anticenter in the plane and a wide swath of high-latitude gas. GALFA's sensitivity, resolution, and sky coverage are thus highly complementary to the IGPS. A great many beautiful cold H ɪ features are visible in GALFA data (e.g., Fig. 9).

Next in line is GASKAP, the Galactic spectral line survey with the Australian SKA Pathfinder (Dickey, this volume). By incorporating new array-feed technology on an interferometer, ASKAP combines the field-of-view of small dishes like DRAO with better resolution, speed, and bandwidth — enough to capture both H ɪ and OH emission, so that the CNM and a hitherto elusive tracer of the molecular medium can be surveyed together for the first time. GASKAP will image the whole Galactic plane within $|b| < 10°$ and $\delta < +40°$ at $10 - 20''$ resolution, yeilding an unprecedentedly rich panorama of the dynamic ISM in our home galaxy. Further down the road, the SKA will enable sensitive H ɪ imaging at few-arcsecond scales, matching photographic sky surveys at last, and enabling studies of nearby Galaxies at the same level of detail the IGPS pioneered for the Milky Way. Both ASKAP and the SKA will also be HICA machines, capturing a huge grid of gas measurements that will revolutionize our view of the Galaxy yet again. The future looks very bright for studies of "dark" gas!
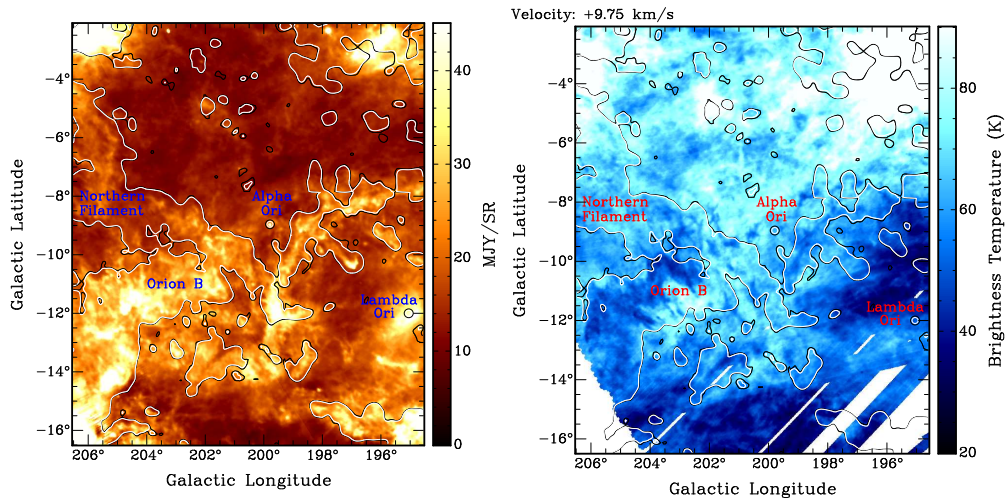
Figure 9.   The northeast part of Orion. *Left:* IRAS 100 μm dust emission; *Right:* GALFA H I at +10 km/s (not fully mapped). Contours are CfA CO 1-0 line integral at 1 K km/s. Stars α and λ Ori are marked, as are the Ori B and N. Filament molecular complexes; the $\sim 8°$ diameter λ Ori molecular ring can also be seen. Richly-detailed HISA is visible in many CO clouds and outside a few (e.g., near α Ori). HISA has been detected previously in this region (McCutcheon et al. 1978; Wannier et al. 1983; Sandqvist et al. 1988; Li & Goldsmith 2003) but has never been imaged as above.

References

Abdo, A. A., Ackermann, M., Ajello, M., & et al. 2010, ApJ, 710, 133

Anderson, L. D., & Bania, T. M. 2009, ApJ, 690, 706

Andersson, B.-G., & Potter, S. B. 2005, MNRAS, 640, 51

Baker, P. L., & Burton, W. B. 1979, A&AS, 35, 129

Bakes, E. L. O., & Tielens, A. G. G. M. 1994, ApJ, 427, 822

Bania, T. M., & Lockman, F. J. 1984, ApJS, 54, 513

Bergin, E. A., Hartmann, L. W., Raymond, J. C., & Ballesteros-Paredes, J. 2004, ApJ, 612, 912

Bergin, E. A., & Tafalla, M. 2007, ARA&A, 45, 339

Braun, R., Thilker, D. A., Walterbos, R. A. M., & Corbelli, E. 2009, ApJ, 695, 937

Busfield, A. L., Purcell, C. R., Hoare, M. G., Lumsden, S. L., Moore, T. J. T., & Oudmaijer, R. D. 2006, MNRAS, 366, 1096

Cao, Y., Terebey, S., Prince, T. A., & Beichman, C. A. 1997, ApJS, 111, 387

Chandrasekhar, S., & Fermi, E. 1953, ApJ, 118, 116

Clark, B. G. 1965, ApJ, 142, 1398

Cox, D. P. 2005, ARA&A, 43, 337

Dame, T. M., Hartmann, D., & Thaddeus, P. 2001, ApJ, 547, 792

Dickey, J. M. 2002, in Single-Dish Radio Astronomy: Techniques and Applications, edited by S. Stanmirović, D. Altschuler, P. Goldsmith, & C. Salter (San Francisco: ASP), vol. 278 of ASP Conf. Ser., 209

Dickey, J. M., & Lockman, F. J. 1990, ARA&A, 28, 215

Dickey, J. M., McClure-Griffiths, N. M., Gaensler, B. M., & Green, A. J. 2003, ApJ, 585, 801

Dickey, J. M., Strasser, S. T., Gaensler, B. M., Haverkorn, M., Kavars, D., McClure-Griffiths, N. M., Stil, J. M., & Taylor, A. R. 2009, ApJ, 693, 1250

Dobbs, C. L., Bonnell, I. A., & Pringle, J. E. 2006, MNRAS, 371, 1663

Dobbs, C. L., Glover, S. C. O., Clark, P. C., & Klessen, R. S. 2008, MNRAS, 389, 1097

Douglas, K. A., Acreman, D. M., Dobbs, C. L., & Brunt, C. M. 2010, MNRAS accepted, 0, 0

Douglas, K. A., & Taylor, A. R. 2007, ApJ, 659, 426

Dwarakanath, K. S., Carilli, C. L., & Goss, W. M. 2002, ApJ, 567, 904

Gazol, A., Luis, L., & Kim, J. 2009, ApJ, 693, 656

Gazol, A., Vázquez-Semadeni, E., & Kim, J. 2005, ApJ, 630, 911

Gazol, A., Vázquez-Semadeni, E., Sánchez-Salcedo, F. J., & Scalo, J. 2001, ApJL, 557, 121

Gibson, S. J. 2002, in Seeing Through the Dust: The Detection of H I and the Exploration of the ISM in Galaxies, edited by A. R. Taylor, T. L. Landecker, & A. G. Willis (San Francisco: ASP), vol. 276 of ASP Conf. Ser., 235

— 2006, BAAS, 38, 124

Gibson, S. J., Taylor, A. R., Dewdney, P. E., & Higgs, L. A. 2000, ApJ, 540, 851

Gibson, S. J., Taylor, A. R., Higgs, L. A., Dewdney, P. E., & Brunt, C. M. 2005a, ApJ, 626, 214

— 2005b, ApJ, 626, 195

Gibson, S. J., Taylor, A. R., Stil, J. M., Brunt, C. M., Kavars, D. W., & Dickey, J. M. 2007, in Triggered Star Formation in a Turbulent ISM, edited by B. G. Elmegreen, & J. Palous (Cambridge: CUP), vol. 237 of IAU Symp., 363

Gibson, S. J., Taylor, A. R., Stil, J. M., Higgs, L. A., Dewdney, P. E., & Brunt, C. M. 2004, in How Does the Galaxy Work? A Galactic Tertulia with Don Cox and Ron Reynolds, edited by E. J. Alfaro, E. Pérez, & J. Franco (Dordrecht: Kluwer), vol. 1, 47

Goerigk, W., Mebold, U., Reif, K., Kalberla, P. M. W., & Velden, L. 1983, A&A, 120, 63

Goldsmith, P. F., & Li, D. 2005, ApJ, 622, 938

Goldsmith, P. F., Li, D., & Krčo, M. 2007, ApJ, 654, 273

Gooch, R. 1996, in Astronomical Data Analysis Software and Systems V, edited by G. H. Jacoby, & J. Barnes (San Francisco: ASP), vol. 101 of ASP Conf. Ser., 80

Grenier, I. A., Casandjian, J.-M., & Terrier, R. 2005, Science, 307, 1292

Habart, E., Boulanger, F., Verstraete, L., Walmsley, C. M., & Pineau des Forêts, G. 2004, A&A, 414, 531

Hasegawa, T., Sato, F., & Fukui, Y. 1983, AJ, 88, 658

Haud, U. 2010, A&A, 514, 27

Heiles, C. 2000, AJ, 119, 923

— 2001, ApJL, 551, 105

Heiles, C., & Troland, T. H. 2003, ApJ, 586, 1067

Hennebelle, P., & Audit, E. 2007, A&A, 465, 431

Hennebelle, P., Audit, E., & Miville-Deschênes, M.-A. 2007, A&A, 465, 445

Hennebelle, P., Banerjee, R., Vázquez-Semadeni, E., Klessen, R. S., & Audit, E. 2008, A&A, 486, 43

Heyer, M. H., Brunt, C., Snell, R. L., Howe, J. E., Schloerb, F. P., & Carpenter, J. M. 1998, ApJS, 115, 241

Heyer, M. H., & Terebey, S. 1998, ApJ, 502, 265

Higgs, L. A. 1999, in New Perspectives on the Interstellar Medium, edited by A. R. Taylor, T. L. Landecker, & G. Joncas (San Francisco: ASP), vol. 168 of ASP Conf. Ser., 15

Higgs, L. A., Landecker, T. L., Asgekar, A., Davison, O. S., Rothwell, T. A., & Yar-Uyaniker, A. 2005, AJ, 129, 2750

Hosokawa, T., & Inutsuka, S.-I. 2007, ApJ, 664, 363

Jackson, J. M., Bania, T. M., Simon, R., Kolpak, M., Clemens, D. P., & Heyer, M. 2002, ApJL, 566, 81

Kalberla, P. M. W., & Kerp, J. 2009, ARA&A, 47, 27

Kavars, D. W., Dickey, J. M., McClure-Griffiths, N. M., Gaensler, B. M., & Green, A. J. 2003, ApJ, 598, 1048

— 2005, ApJ, 626, 887

Kerton, C. R. 2005, ApJ, 623, 235

Kerton, C. R., & Martin, P. G. 2000, ApJS, 126, 85

Kim, C.-G., Kim, W.-T., & Ostriker, E. C. 2006, ApJL, 649, 13

— 2008, ApJ, 681, 1148

Klaassen, P. D., Plume, R., Gibson, S. J., Taylor, A. R., & Brunt, C. M. 2005, ApJ, 631, 1001

Knapp, G. R. 1974a, AJ, 79, 541

— 1974b, AJ, 79, 527

Knapp, G. R., & Verschuur, G. L. 1972, AJ, 77, 717

Knee, L. B. G., & Brunt, C. M. 2001, Nature, 412, 308

Koyama, H., & Inutsuka, S.-I. 2000, ApJ, 532, 980

Kulkarni, S. R., & Heiles, C. 1988, in Galactic and Extragalactic Radio Astronomy (2nd Ed), edited by G. L. Verschuur, & K. I. Kellermann (New York: Springer-Verlag), vol. 1, 95

Landecker, T. L., Roger, R. S., & Higgs, L. A. 1980, A&AS, 39, 133

Li, D., & Goldsmith, P. F. 2003, ApJ, 585, 823

Liszt, H. S. 2001, A&A, 371, 698

Lupton, R. H., & Monger, P. 1997, The SM Reference Manual (Princeton: www.astro.princeton.edu/ rhl/sm)

McClure-Griffiths, N. M., Dickey, J. M., Gaensler, B. M., Green, A. J., & Haverkorn, M. 2006, ApJ, 652, 1339

McClure-Griffiths, N. M., Dickey, J. M., Gaensler, B. M., Green, A. J., Haverkorn, M., & Strasser, S. 2005, ApJS, 158, 178

McClure-Griffiths, N. M., Dickey, J. M., Gaensler, B. M., Green, A. J., Haynes, R. F., & Wieringa, M. H. 2001, PASA, 18, 84

McCutcheon, W. H., Shuter, W. L. H., & Booth, R. S. 1978, MNRAS, 185, 755

Micelotta, E. R., Jones, A. P., & Tielens, A. G. G. M. 2010, A&A, 510, 36

Minter, A. H., Lockman, F. J., Langston, G. I., & Lockman, J. A. 2001, ApJ, 555, 868

O'Halloran, B., Satyapal, S., & Dudik, R. P. 2006, ApJ, 641, 795

Poppel, W. G. L., Marronetti, P., & Benaglia, P. 1994, A&A, 287, 601

Radhakrishnan, V., Murray, J. D., Lockhart, P., & Whittle, R. P. J. 1972, ApJS, 24, 15

Reach, W. T., Koo, B.-C., & Heiles, C. 1994, ApJ, 429, 672

Riegel, K. W., & Crutcher, R. M. 1972, A&A, 18, 55

Roberts, W. W. 1969, ApJ, 158, 123

— 1972, ApJ, 173, 259

Roman-Duval, J., Jackson, J. M., Heyer, M., Johnson, A., Rathborne, J., Shah, R., & Simon, R. 2009, ApJ, 699, 1153

Sandqvist, A., Tomboulides, H., & Lindblad, P. O. 1988, A&A, 205, 225

Sato, F., Whiteoak, J. B., Otrupcek, R. E., & Tokushige, T. 1992, AJ, 103, 1627

Sheffer, Y., Rogers, M., Federman, S. R., Abel, N. P., Gredel, R., Lambert, D. L., & Shaw, G. 2008, ApJ, 687, 1075

Snow, T. P., & McCall, B. J. 2006, ARA&A, 44, 367

Spitzer, J., L. 1978, Physical Processes in the Interstellar Medium (New York: Wiley)

Stil, J. M., Taylor, A. R., Dickey, J. M., & et al. 2006, AJ, 132, 1158

Strasser, S., & Taylor, A. R. 2004, ApJ, 603, 560

Strasser, S. T., Dickey, J. M., Taylor, A. R., & et al. 2007, AJ, 134, 2252

Taylor, A. R., Gibson, S. J., Peracaula, M., & et al. 2003, AJ, 125, 3145

Taylor, J. H., & Cordes, J. M. 1993, ApJ, 411, 674

van der Werf, P. P., Dewdney, P. E., Goss, W. M., & Vanden Bout, P. A. 1989, A&A, 216, 215

Vázquez-Semadeni, E., Gilberto C. Gómez, G. C., Jappsen, A. K., Ballesteros-Paredes, J., González, R. F., & Klessen, R. S. 2007, ApJ, 657, 883

Vázquez-Semadeni, E., Ryu, D., Passot, T., González, R. F., & Gazol, A. 2006, ApJ, 643, 245

Verschuur, G. L., & Schmelz, J. T. 1989, AJ, 98, 267

Wannier, P. G., Lichten, S. M., & Morris, M. 1983, ApJ, 268, 727

Wendker, H. J., Schramm, K. J., & Dieckvoss, C. 1983, A&A, 121, 69

Westerhout, G., & Wendlandt, H.-U. 1982, A&AS, 49, 143

Wolfire, M. G., Hollenbach, D., & McKee, C. F. 2010, ApJ, 716, 1191

Wolfire, M. G., Hollenbach, D., McKee, C. F., Tielens, A. G. G. M., & Bakes, E. L. O. 1995, ApJ, 443, 152

Wolfire, M. G., McKee, C. F., Hollenbach, D., & Tielens, A. G. G. M. 2003, ApJ, 587, 278